Zero volt storage of Na-ion batteries: Performance dependence on cell chemistry!

Parth Desai,[1,2,3] Jiaqiang Huang,[1,3] Dominique Foix,[4] Jean-Marie Tarascon[1,2,3,] and Sathiya Mariyappan.[1,3,**]*

[1]Chimie du Solide-Energie, UMR 8260, Collège de France, 75231 Paris Cedex 05, France
[2]Sorbonne Université, 4 Place Jussieu, 75005, Paris, France
[3]Réseau sur le Stockage Electrochimique de l'Energie (RS2E), FR CNRS 3459, France
[4]IPREM, CNRS, Université de Pau & Pays Adour, E2S-UPPA, Hélioparc, 2 Avenue P.Angot, 64053 Pau Cedex 9, France
*Correspondence: jean-marie.tarascon@college-de-france.fr
**Correspondence: sathiya.mariyappan@college-de-france.fr

ABSTRACT

Sodium-ion batteries (NIBs) are regaining their importance in recent years as a sustainable complementary energy storage device for Li-ion batteries. Although, they cannot compete in terms of energy density with respect to Li-ion, they present a few advantages, namely the 0V stability that makes them safe during external short and/ or over-discharge. When the cell is discharged to 0V, the negative electrode potential shoots up high during which the copper current collector in use for Li-ion cells could oxidize, dissolve and leads to internal short. In contrast Na-ion cells utilize aluminium current collector that is strongly resistant against oxidation, hence enabling their 0V stability. However, apart from the current collector stability, the negative electrode potential rise could cause interphase instability which is not well elucidated. Hence, herein, we explored two different Na-ion chemistries, namely polyanionic $Na_3V_2(PO_4)_2F_3$-hard carbon and sodium layered oxide-hard carbon using different electrolyte formulations. Combined impedance analyses, *ex-situ* X-ray photoelectron spectroscopy (XPS) and operando optical sensing indicate the 0V discharge involves SEI degradation thereby deteriorating the cell performance, extent of which depends on the positive electrode potential and the electrolyte in use. Overall, the 0V stability is not an in-built property of Na-ion cells and a careful selection of cell chemistry is mandatory to achieve 0V stable Na-ion cells.

Key words: Na-ion cells, 0V stability, solid-electrolyte interphase stability, operando optical calorimetry, X-ray photoelectron spectroscopy.

INTRODUCTION

In the last two decades, lithium-ion batteries (LIBs) have dominated the energy storage devices market. Numerous advantages like low cost, high voltage and superior energy density make LIBs an irreplaceable commodity.[1] Owing to its versatile nature, LIBs have expanded their portfolio from portable electronic devices to electric vehicles (EVs) and smart grids.[2] Bearing in mind that the production of LIBs is mainly concentrated in East Asia, safe transportation of these cells to the majority of the end users is of paramount importance. Owing to safety risks stemming from their flammable liquid electrolytes, LIBs are declared as "dangerous goods" by International Civil Aviation Organization (ICAO) and United Nations Economic Commission for Europe (UNECE). Thus, various restrictions are then imposed on their shipping[3] and are advised to be transported by regulating the maximum state of charge (SOC) to 30%.[4]

Even after all these tests and safety regulations, we count nearly *354* incidents(over the last 15 years)[5] of fire, smoke, or explosion of LIBs carried by cargo or air with some of them being caused by unintentional external shorts of the cells. During external short, the cell reaches 0V, where the negative electrode is pushed to high potentials to match the positive electrode's potential. During this process, the copper current collector in the negative electrode also reaches a high potential that eventually oxidizes (Fig. S1), leading to Cu-dissolution that can trigger the growth of Cu dendrites and internal short.[6], [7] In contrast, Na-ion batteries (NIBs) are assembled with an aluminum (Al) current collector which is quite more stable than Cu towards oxidation (Fig. S1), as sodium does not form an alloy with aluminium unlike lithium.[8][9] Hence, some papers and a patent from Faradion Limited state that their NIBs containing sodium transition metal layered oxide as the positive electrode and hard carbon (HC) as the negative electrode can be safely shipped in their shorted (0V) state.[10][11]

Thus, the legitimate question is, whether solely the current collector stability determines the 0V stability of the cell? If so, besides layered oxide chemistry, there are two other Na-ion chemistries on the verge of commercialization, namely the polyanionic $Na_3V_2(PO_4)_2F_3$ (NVPF)-hard carbon (HC) developed by the start-up TIAMAT in France, Prussian blue analogs- hard carbon one pursued by both Natron (USA) and CATL (China), respectively.[12],[13],[14] In this

case, whether the reported 0V stability of Na-ion cell is true and extendable for these chemistries as well?

To answer these questions, we first studied the Li-ion cells consist of $LiNi_{0.8}Mn_{0.1}Co_{0.1}O_2$ (NMC811)–graphite and $LiFePO_4$ (LFP)-graphite electrodes for 0V stability, as a benchmark system. Following, to analyze the 0V stability of Na-ion cells, we first selected the $Na_3V_2(PO_4)_2F_3$ (NVPF) and hard carbon (HC) system that we are developing with TIAMAT. Let's recall that HC is a cheap and ideal negative electrode material for NIBs with around ~300mAh/g of reversible capacity with an average voltage of 0.13V vs. Na/Na^+. NVPF has a higher average discharge potential of 3.7V than 3.1V (vs. Na/Na^+) reported for several sodium layered oxides,[15] hence allowing the possibility to study the role of positive electrode potential in 0V stability. Moreover, with a material-level specific energy of ~420 Wh/kg and the structural stability upon long cycling, NVPF-HC chemistry will even be more attractive from an application point of view if such chemistry could also exhibit 0V stability, like what has been reported by Faradion[8] using layered oxides rather than NVPF.

By monitoring the solid electrolyte interphase (SEI) evolutions on $Na_3V_2(PO_4)_2F_3$-HC cells via complementary cyclic-voltammetry, impedance analyses, operando optical heat calorimetry, and X-ray photoelectron spectroscopy (XPS), we present evidence for SEI degradation during 0V discharge and the loss of Na inventory for SEI reformation upon subsequent cycling. Finally, we provide means of improving the 0V stability of NVPF-HC cells by tuning the electrode/ electrolyte formulations or even by moving to sodium layered oxide $NaNi_{0.45}Zn_{0.05}Mn_{0.35}Ti_{0.15}O_2$ (ZNMT))-HC system.

EXPERIMENTAL PROCEDURES

Electrochemical analyses: All electrochemical tests were carried out using either MPG2 potentiostat or BCS battery cycler (Bio-Logic, France). Four different cell configurations are used in the manuscript to compare Li- and Na-ion cells. The mainly studied cell configurations are, (i) $LiNi_{0.8}Mn_{0.1}Co_{0.1}O_2$ // 1M $LiPF_6$ in ethylene carbonate (EC)-dimethyl carbonate (DMC) (1:1) // Graphite, (ii) $LiFePO_4$ // 1M $LiPF_6$ in EC-DMC (1:1) // Graphite, (iii) $Na_3V_2(PO_4)_2F_3$ // 1M $NaPF_6$ in EC-propylene carbonate (PC)-DMC (1:1:1) // Hard carbon and (iv) O3 $NaNi_{0.45}Zn_{0.05}Mn_{0.35}Ti_{0.15}O_2$

// 1M $NaPF_6$ in EC-PC-DMC (1:1:1) // Hard carbon. In all these configurations, the active material is mixed with conducting carbon and coated on Cu (graphite) or Al (all other materials) foil using polyvinylidene fluoride (PVDF) binder. The active material masses for positive and negative electrodes were balanced considering their practical capacities with the negative to positive (n/p) ratio of 1.1. The electrodes are punched into 11 mm diameter for studies in Swagelok type cells and 12.7 mm diameter for 2032 coin cells. The electrodes are dried at 80°C in a vacuum and transferred to argon filled glove box where the cell assemblies were carried out. The electrolytes were homemade by dissolving the dry $LiPF_6$/ $NaPF_6$ in mentioned solvent(s). The solvents used in this study are battery grade EC, PC, DMC etc, purchased from E-lyte, Germany. The solvents were dried over molecular sieves and tested for water content using Karlfisher titration. The water content was always less than 10ppm in the used solvents.

Two types of cell designs were used. (i) *Three electrode cells:* Swagelok type three electrode cells were used for the analyses. Lithium metal is used as a reference electrode for Li-ion cells and $Na_3V_2(PO_4)_3$ charged to 3.4V (50% state of charge) is used as a reference electrode for Na-ion cells. Tests were carried out at either C/10 or C/5 rates at 25 °C.

(ii) *Full cells testing: The Li (Na)-ion cells assembled using* insertion electrodes for both positive and negative electrodes (vs. Li(Na)- metal as a negative electrode in Li(Na)-half cell) are termed as full cells throughout the manuscript. The long cycle performance of different electrodes with or without 0V hold was measured in coin type 2032- cells. The dried electrodes were separated by two layers of glass fiber containing 150 µL of desired electrolytes.

Electrochemical Impedance Spectroscopy (EIS) measurements: The impedance spectra were collected in coin cells, over a frequency range of 20 kHz to 10 mHz with six points per decade and a perturbation amplitude of 10 mV. Two cells were assembled for each experiment to confirm the reproducibility of the impedance data and measurements were done at 25°C.

X-ray photoelectron spectroscopy analyses: X-ray photoemission spectroscopy (XPS) measurements were carried out with a THERMO Escalab spectrometer, using focused monochromatic Al Kα radiation (hν = 1486.6 eV) and equipped with an argon-filled glove box. The HC samples were cycled using the prescribed condition and removed at 2V, washed using

dry DMC and sealed in argon. The samples were preserved from moisture and air at all times from their preparation to their analysis. Peaks were recorded with a constant pass energy of 20 eV. The pressure in the analysis chamber was around 5×10^{-8} mbar. The binding energy scale was calibrated using the C 1s peak at 285.0 eV from the hydrocarbon contamination present at the surface of the sample. The spectra were fitted using a minimum number of components. Several spectra were recorded at different times to check that the samples were not subjected to degradation during the X-ray irradiation.

Operando optical calorimetric analyses: Hermetically sealed NVPF/HC cylindrical 18650 cells without electrolyte were received from Tiamat, France. A 0.8 mm diameter hole was drilled into the negative pole of the dry, 18650 cells. The position was selected according to the welding point of the negative current collector, which was close to the centre of the negative pole. This choice of position helped in avoiding the destruction of the jelly roll and in preventing the strain interaction between the TFBG sensors and the jelly roll. All of the 18650 cells were dried in a Buchi oven under vacuum at 80 °C for 12 h prior to being transferred into the glovebox. The 18650 cells were then filled with 5.5 mL of the desired electrolyte inside the glovebox. Then the FBG sensors were inserted into the central void of the jelly roll through the drilled hole using a needle. The interface between the needle containing the TFBG sensor and the 18650 cell was subsequently sealed with an epoxy that was cured for 24 h; all processes were performed inside the glove box whose O_2 and H_2O content was maintained at less than 0.1 ppm. Cells were cycled using BCS battery cycler (Bio-Logic, France) by keeping the cells inside an oven at 55 °C, and the cycling rates were calculated on the basis of NVPF material (1C = 128 mA g^{-1}). Sensors were connected to FBGuard1550 (Safibra) or LUNA Si255 (Micron Optics) interrogator via optical fibers. The sampling period of the interrogator was set to 1 s. According to the mentioned specifications, the wavelength accuracy of the interrogators is 1 pm. The FBGs were purchased from SAMYON and calibrated before use. The temperature calibration of the FBG sensors was conducted as reported previously.[16][17][18]

RESULTS AND DISCUSSIONS

1. Benchmark system: Li-ion cells towards 0V storage

To study the 0V behavior of LIBs, coin type cells were assembled using $LiNi_{0.8}Mn_{0.1}Co_{0.1}O_2$ – graphite and $LiFePO_4$ -graphite having Al and Cu as the positive and negative current collector, respectively. The cycling stability of the cells during 0V hold is tested using a quite harsh cycling protocol (Fig. S2) that consists of 5 cycles over the 3- 4.2V voltage window followed by pushing the discharge voltage to 0V for 24h or 72h (0V hold), and repeating the 5 cycles - 0V holds, continuously until the cell deteriorates completely. The cells without any 0V hold were also tested for a rational comparison. A gain in capacity (Figure 1a and 1b) is observed after each 0V holding, however, the capacity decreases upon subsequent cycling and the capacity decay is faster in the cells with 0V hold than in the cells without 0V holding. For NMC811-graphite, the cells rapidly fail after three 0V holds, as compared to six holds for a LFP-graphite cells, indicative of a slower degradation for LFP-based cells.

To understand this difference, three-electrode cells were built using Li-metal as the reference electrode, and the cycling profile of each electrode was followed separately. Noteworthy is the graphite potential that shoots up to 3.53 V *vs*. Li/Li^+ when the NMC811- graphite cell goes to 0V. At such potential oxidation-driven dissolution of copper is visualized on the separator when disassembling the cell (Fig. S3). This dissolved copper can then reduce leading to metallic deposits on the negative and positive electrodes that could damage the electrode-electrolyte interphase (EEI), leading to rapid capacity loss and cell failure. In case of multiple over-discharges to 0V, the deposited Cu can form dendrites[19] creating internal short and thermal runaway.

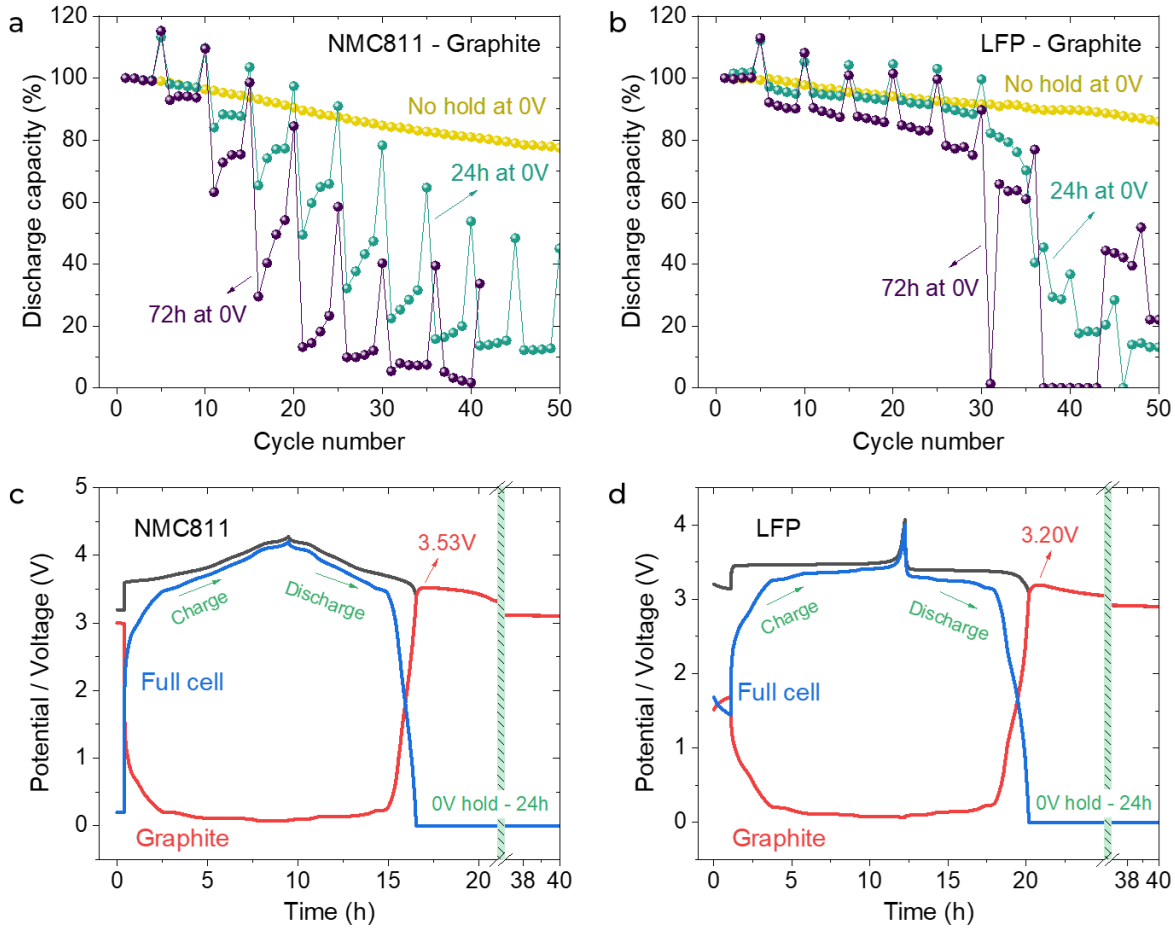

Figure 1. *Discharge capacity vs. cycle number of (a) LiNMC811- Graphite and (b) LFP- Graphite cells. Three different cycling conditions were compared for cells cycled without any 0V holding, with 24h and 72h holding for every 5 cycles. Cycling profile of (c) LiNMC811- graphite and (d) LFP- graphite in three electrode cell assembly where lithium metal is used as the reference electrode.*

In contrast, the graphite potential in LFP- graphite cells shoots up to a lower value of 3.2V *vs*. Li/Li^+ (shown in Figure 1d) during 0V hold. Hence, the cell degradation in LFP- graphite in the initial 0V holds can mainly be ascribed to a degradation of the solid-electrolyte interphase (SEI) at the graphite negative electrode. However, upon repetitive 0V storage, it leads to larger cell polarization (Fig. S4), and therefore a higher potential shoot-up of graphite electrode and subsequent Cu dissolution as discussed before. Overall, both NMC811- graphite and LFP-graphite cells containing Cu as a current collector for graphite show rollover type failure (sudden death of the cell)[20] on a few 0V-holds and cycling.

2. Sodium-ion cells at 0V

2.1 SEI decomposition and regrowth

The NVPF-HC full cell cycling stability in 2032 coin type cells, using the same protocol as studied above, is shown in Figure 2a for comparison, with the behavior of a similar cell but without 0V hold. The normalized cell polarization evolution for all the cells was calculated as described in the supporting note. 1 is shown in Figure 2b. Faster capacity degradation (Figure 2a) together with an increase in cell polarization (Figure 2b) is observed for cells with 0V hold. Still, there is no appearance of a sudden cell death/ rollover failure, as is the case with Li-ion batteries, as shown in Figure 1.

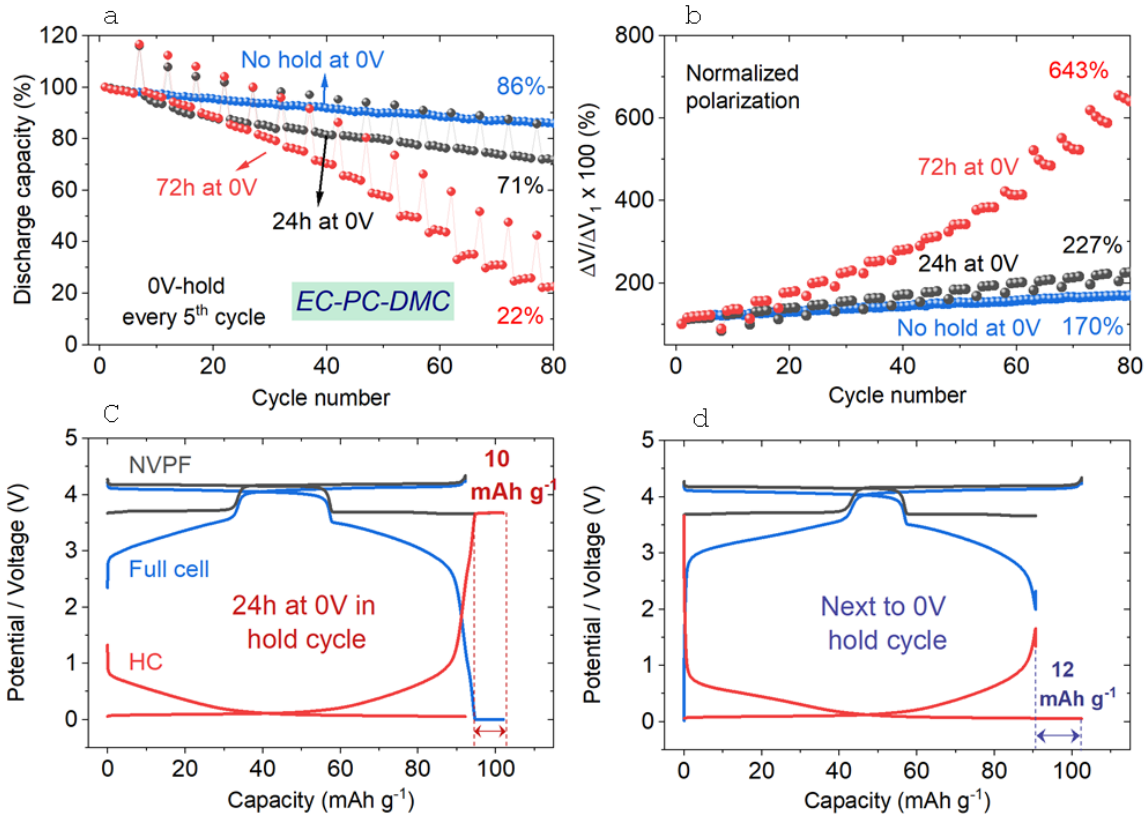

Figure 2. *(a) Capacity retention (%) and (b) normalized polarization as a function of cycle number of NVPF-HC cells using 1M $NaPF_6$ in EC-PC-DMC electrolyte. Cell formation with two cycles was done at 55°C leading to 25% irreversible loss in the first cycle. (c-d) Cycling profile of NVPF-HC Na-ion cells in three electrode set-up using NVP at 50%SOC as reference electrode, (c) during 0V discharge with 24h holding at 0V and (d) on subsequent charge. The actual potentials were calculated vs NVP and converted vs Na/Na^+ using the conversion factor xV vs NVP= (x+ 3.37) V vs Na/Na^+, as NVP reference electrode is used at 3.37 vs Na/Na^+.*

In parallel, the three electrode measurements using $Na_3V_2(PO_4)_3$ (NVP) with 50% SOC as the reference electrode indicate that the hard carbon potential is raised to 3.67 V vs. Na/Na^+ (~0.96 V vs. standard hydrogen electrode (SHE)) while discharging the NVPF-HC cell to 0V (Figure 2c). This potential is higher than the potential for the LiNMC811-Graphite cells (3.53 V vs. Li^+/Li, ~0.49 V vs. SHE). Hence the observed stability of NVPF-HC cells with repeated 0V holding against the Li-ion cells could be due to the stability of the Al current collector, which is stable up to 4.5 V *vs*. Na/Na^+ in PF_6^- based electrolytes (Fig. S1).

Turning back, Figure 2a shows an increase in discharge capacity upon each holding of the cells at 0V for 24h or 72h. Such an increase in capacity upon 0V holding is much higher than what we could observe for a 2V or 1V holding (Fig. S5). It indicates that the observed capacity raise during 0V hold is not solely related to Na^+ diffusion kinetics. Interestingly, holding the cells at -1V leads to a much higher increase in capacity implying extra Na-insertion into NVPF structure (Fig. S5). It is important to mention that the maximum observed increase in capacity is equivalent to the first cycle irreversibility of the NVPF-HC cells (the maximum sodium re-inserted into the NVPF structure never increased beyond 3). Since there is no extra Na-inventory in a full cell, we expect that the hard carbon is fully de-sodiated at this potential (~2V or less) and the observed gain in capacity (Na^+ to insert into NVPF) must be related to the SEI decomposition. Additionally, our cyclic voltammetry studies (Fig. S6) confirm that the formed SEI has poor oxidative stability and starts to oxidize above 2.5 V (vs. Na/Na^+). Upon recharge (Figure 2d), the gained 12mAh/g is lost from the HC electrode to reform the SEI, evident from the HC curve during discharge.

2.2 Probing SEI film resistance

Impedance spectroscopy was used next to interrogate the dynamic of the SEI during 0V hold. The NVPF-HC cell was cycled and impedance spectra were collected for each charge and discharge till 2V with intermittent 0V-hold for 24h (Figure 3a) on every one cycle. We mainly analyzed the impedance spectra collected at 2V in order to minimize the contribution from charge transfer resistance and to solely track the changes with the interphase film resistances (Fig. S7). [23]

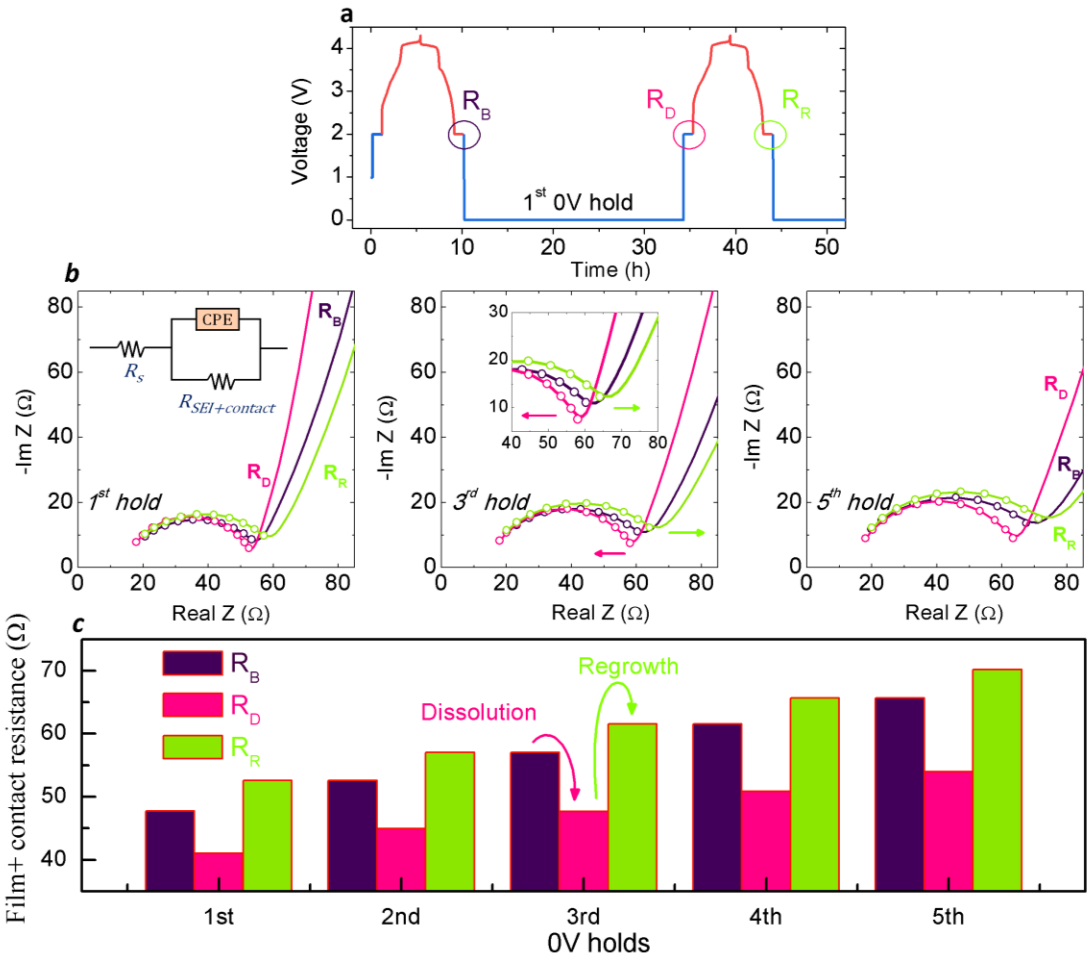

Figure 3. *(a) The cycling condition followed to study the impedance spectra where the impedance analysis was carried out at 2V before 0V hold (R_B), charge after 0V hold (R_D) and the next cycle (R_R). The spectra in (b) cumulates these impedance spectra after 1(left), 3(middle) and 5(right) holds at 0V for 24h. Equivalent circuit model is represented in inset of left figure in (b). The dots on the semicircle part of the impedance curves are from the fitted data while the solid line represents the experimental data. (c) The impedance value obtained by fitting the spectra using the equivalent circuit shown in (b). In this regard, note that the R_R for n^{th} cycle becomes the R_B for the $(n+1)^{th}$ cycle and so on. The decrease in impedance during 0V hold is shown as 'dissolution' and the increasing impedance during SEI reformation is mentioned as 'regrowth' in the figure.*

As an illustration the impedance spectra before and after 0V hold together with one cycle after 0V hold, corresponding to the first, third, and fifth 0V-hold are represented in Figure 3b (Nyquist plot) and in Fig. S8 (Bode plot). The semicircle part of impedance spectra is of importance to track SEI film resistance, which is fitted using the model in Fig. 3b inset (left) and represented by dots on the impedance curves. The resistance measured before and after 0V hold, and one cycle

after 0V hold are defined as (R_B), (R_D) and (R_R), respectively. The interphase resistances calculated using the equivalent circuit shown in Fig. 3b inset (left) is shown in Figure 3c as a function of 0V hold cycles. There is a decrease in interphase film resistance during the 0V-hold ($R_D < R_B$), indicating interphase degradation-dissolution, and a resistance increase after the next cycle ($R_B < R_R$), suggesting its reformation. The trend $R_D < R_B < R_R$ observed throughout all the holds confirms the interphase dissolution-reformation mechanism with increasing resistance during the reformation step. It indicates parasitic reactions during the interphase reformation. This repeated sequence is damaging for the cell since it results in a significant impedance rise, around a 40% increase in resistance between the first and fifth 0V hold. The electrode materials (HC and NVPF) analyzed after impedance by XRD and SEM indicate less modification in the bulk material level, hence the observed degradation mainly comes from interphase instability (Fig. S9 and S10).

2.3. Ex-situ XPS analyses of the interphases:

In order to follow the interphase evolution during the 0V hold process in positive and negative electrodes separately, we, next interrogate the NVPF and HC electrodes by X-ray photoelectron spectroscopy (XPS). The XPS spectra of the NVPF pristine and cycled electrodes (Fig. S11) at different stages of the 0V hold process remain unaltered, indicating the absence of significant change in the cathode electrolyte interphase (CEI) during 0V hold. This could be explained bearing in mind that the NVPF electrode is maintained at ~3.67V (see Figure 2c) during 0V hold of the NVPF-HC cell, at which the CEI could be stable from oxidation/ reduction. In contrast, the XPS spectra carried out on the pristine HC electrode and on cycled electrodes at the different points indicated in Figure 4a, exhibit huge variation (Figure. 4b) demonstrating the observed changes in interphase during 0V hold mainly come from SEI decomposition and recreation. Since the SEI is known to be composed of organic and inorganic components,[24] we utilize XPS, its evolution in composition through a cycle to understand which of the components are involved in its degradation and reformation.

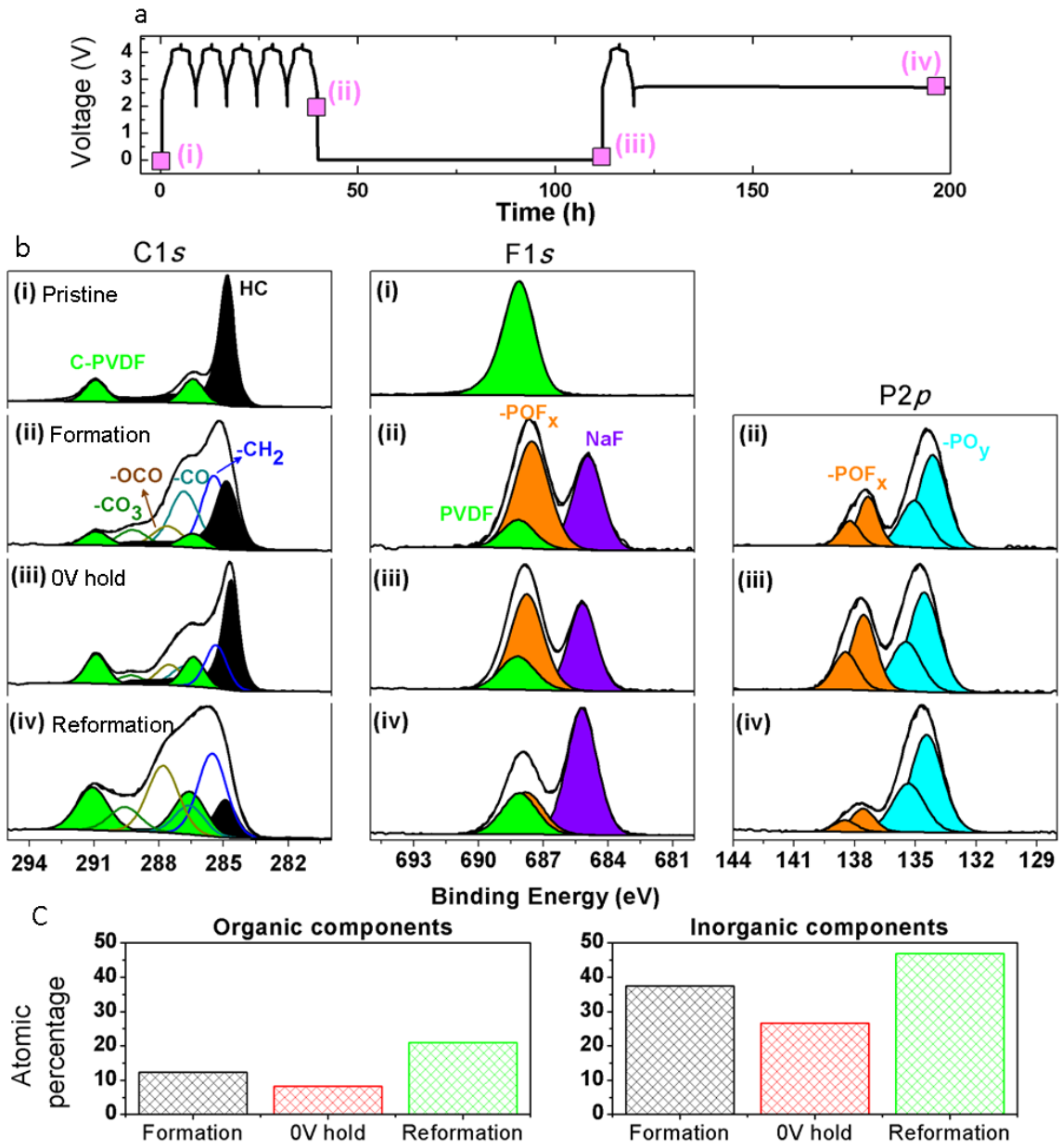

Figure 4. *XPS analyses of the HC electrodes recovered at different states of NVPF-HC cell cycling as per the points mentioned in (a). The C1s, F1s and P2p for all the electrodes are cumulated in (b). There is no P components in the pristine electrode and hence not included in this image. (c) Histogram showing the relative amount of organic and inorganic components of SEI during formation, degradation/dissolution (0V hold) and reformation (one cycle after 0V hold). Noteworthy, the intensity of HC spectrum is less seen whenever there is a SEI growth. Hence, the quantifications of SEI components were done by normalizing C1s peak area of HC as 10 in all the spectra (Table S1).*

The XPS spectra of pristine electrode in Figure 4b(i) exhibit peaks due to only HC and PVDF binder (C and F). After the formation cycle, it additionally shows peaks due to C-O, -CH_2, and

NaF together with decomposed species of $NaPF_6$ (-POF_x and -PO_y), indicating that the SEI is composed of organic (C1s) and inorganic (F1s and P2p) components. The XPS spectra in (iii) and the quantification results in Figure 4c (Table s1)) indicate degradation/ dissolution of SEI upon 0V hold in both organic and inorganic components.[24][25] Upon subsequent cycle, reformation of SEI is observed (iv) and Figure 4c where the intensity of organic and inorganic components is much higher than the initial SEI observed during the formation cycle. This confirms the thickening of the SEI layer during the reformation steps.

Based on all the above observations, we propose (Figure 5) the reaction scheme for 0V hold, where a part of SEI oxidizes/ decompose/ dissolve to provide Na^+ ion to insert into the NVPF structure. Upon subsequent charge after 0V hold, a part of Na^+ from NVPF is used for SEI reformation together with additional electrolyte decomposition. Hence, the reformed SEI is getting thicker, leading to an increase in the SEI impedance that is reflected by a larger cell polarization (Figure 2b).

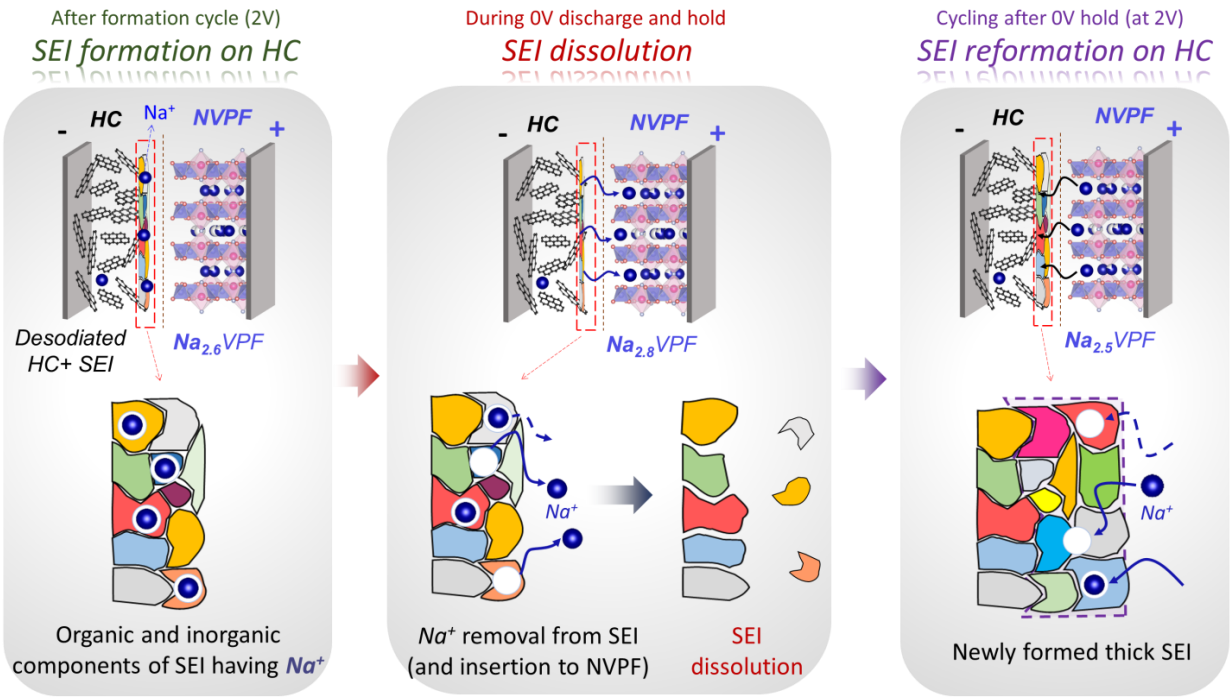

Figure 5. *Schematic showing the SEI formation, dissolution during 0V hold and reformation on subsequent cycle.*

2.4 Operando tracking of heat related to SEI

Now, the question arises, what is the thermal behavior of the Na-ion cell during this 0V hold? Our previous studies using optical calorimetry and other calorimetry analyses in the literature show that both SEI formation and decomposition reactions are associated with heat changes.[16–18] Hence, operando optical calorimetry is performed next to track the heat changes during 0V holding and cycling.

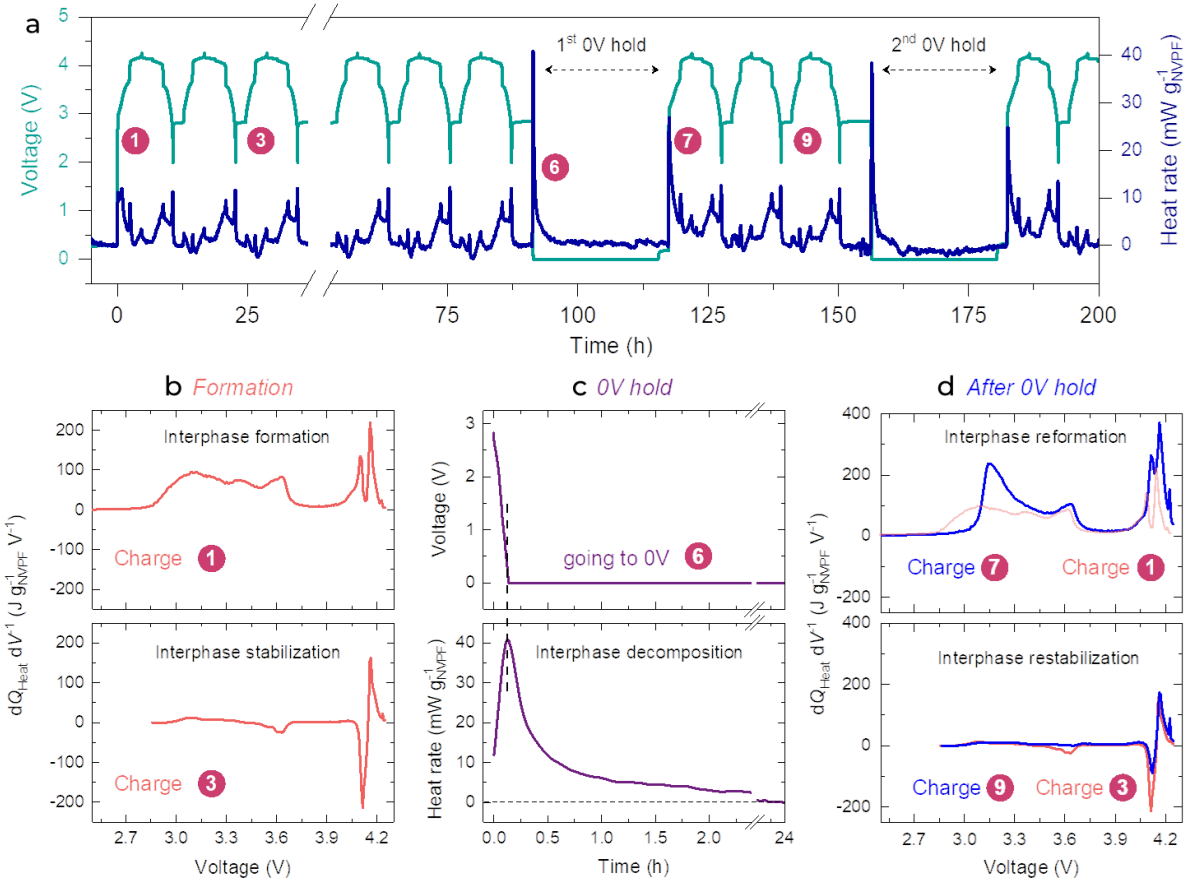

Figure 6. *(a) Heat evolutions for cylindrical 18650 NVPF-HC cells during formation cycle and 0V hold, subsequent cycles measured by TFBGs, the time where break appears in the graph were used for thermal calibration. The heat derivative from charges 1, 3, 6, 7, and 9 (marked in (a)) is shown in (b) formation cycles (c) during 0V hold and (d) SEI recreation after 0V hold.*

Optical calorimetry measurements using tilted fiber Bragg grating (TFBG) sensors inscribed on optical fibers, embedded into dry 18650 NVPF/ HC cells, received from TIAMAT and filled with 1M $NaPF_6$ in EC-PC-DMC electrolyte. Details regarding the integration of TFBG sensors into the

cell together with their calibration were reported in our previous works.[16] The experiments were carried out at 25 °C using a C/5 cycling rate in constant current mode. The shift in Bragg wavelength ($\Delta\lambda_B$) of the TFBGs is followed using an optical interrogator, and the measured $\Delta\lambda_B$ was converted to temperature variations (ΔT) with high resolutions (1s and 0.1°C, respectively).[16],[17] The ΔT, in turn, was used to calculate the heat rate ($\dot{Q} = dQ_{heat}/dt$) and heat derivative (dQ_{heat}/dV) using a simplified 0D thermal mode.[17],[18]

At first, the capacity retention plot (See Fig. S12) shows that the observed increase in capacity during 0V hold and the following deterioration in cycling performances are reproducible in the cylindrical 18650 cells, as is observed with coin cells shown in Figure 2. The heat values derived from the TFBGs are shown in Figure 6a, together with the cell potential evolutions as a function of time. An increase in heat is observed during SEI formation (first cycle charge) as well as during each 0V hold and subsequent charge (Figure 6a). Such an increase in heat indicates that both SEI (re)formation and decomposition are exothermic by nature. This exothermic heat observed in the first charge that is associated with the interfacial reactions[18] decreases abruptly after the formation of stable SEI (charge 3 in Figure 6b). Upon discharging to 0V (Figure 6c), a considerable increase in heat is again observed, reaching the maximum when the cell reaches 0V and decreasing slowly afterward. Still, the heat release never became zero during the whole 24h holding period at 0V, indicating continuous parasitic reactions during this period. Interestingly, exothermic reactions of even greater intensities than during the formation cycle are observed (Figure 6d). This larger heat release suggests that the species involved/ decompose during this SEI reformation most likely differ from the initial formation cycle. It results that this interphase reformation leads to Na-inventory loss and this repeats for all SEI reformation after each 0V hold (Fig. S13), hence explaining the rapid capacity decay observed through this cycling sequence.

In short, although the Al current collector is stable upon 0V discharge of Na-ion cells, all the above studies combined indicate that SEI forming on hard carbon is not very stable at such high oxidation potentials (3.67 V in the case of NVPF-HC cells) hence the need to find means to overcome this stability issue.

3. Optimizing the cell chemistry for better 0V stability of Na-ion cells

At this point, it is important to see whether it is possible to improve the 0V stability of the Na-ion cells. It is known from the literature that the SEI stability depends on the electrolyte formulation since the SEI is created from the reduction of salts, solvents, and additives. Hence, our first approach is to optimize the electrolyte formulation for 0V storage of the Na-ion cells.

3.1 Acting at the electrolyte level

The effect of changing the electrolyte solvent from EC-PC-DMC to different linear and cyclic carbonate combinations or even single solvents on the cycling stability after 0V hold was studied. The capacity retention plots are given in Fig. S14 and the percentage capacity retention after 80 cycles (15 times of 0V hold at 24h) are compared in Figure 7a. The best capacity retention was observed for PC electrolyte (84% after 80 cycles), which also showed a minor increase in polarization (Figure 7b) even by holding at 0V for 72 hours each time. The least stability is observed with DMC based electrolytes (71% after 80 cycles). As discussed in the previous section, SEI dissolution, SEI reformation reactions and subsequent cross talk between both electrodes, will govern the stability of the cells under intermittent 0V storages. It is known from our previous studies that the cross talk species formed after reduction at HC, in presence of PC, are more stable than the DMC/EMC ones for oxidation on NVPF[26], hence explaining the superior stability of PC electrolyte. However, PC alone cannot be used as an electrolyte solvent due to its high viscosity.

Thus, in a subsequent trial we used the electrolyte formulation composed of 1M $NaPF_6$ in EC-PC-DMC having 4 additives namely 3 wt% succinonitrile (SN), 3% vinylene carbonate (VC), 0.5% sodium oxalatodifluoroborate (NaODFB) and tri-methylsilylphosphite (TMSPi) that shows good calender/ cycle life at ambient and high temperatures, as reported previously.[18] An increase in the cell capacity is observed upon 0V hold with similar capacity retention to uninterrupted cycling in the initial stages of 0V holding for 24h or 72h (Figure 7c). However, to our surprise, the cell deteriorated very rapidly after a few 0V holding processes and this was accompanied by a huge increase in impedance (Figure 7c) leading to the cell's rollover failure. Looking back at the 0V degradation mechanism, it seems intuitive that multiple times reduction of additives and

their bi-products (during repetitive 0V storages) will significantly increase the cell's impedance due to thick interphase formation and will lead to Na plating (Fig. S15). Such Na-plating is also re-confirmed in 18650 cells (Fig. S16) indicating that the plating phenomenon is triggered mainly by impedance increase due to 0V storages. This is simply a crucial reminder of the complexity of designing electrolytes that could reunite high temperature performances and 0V stability. A greater in-depth characterization of the SEI decomposition products during 0V holding, combined with multiple experimental screening and trials is still needed for designing an optimized multi-purpose electrolyte for NVPF/HC Na-ion cells.

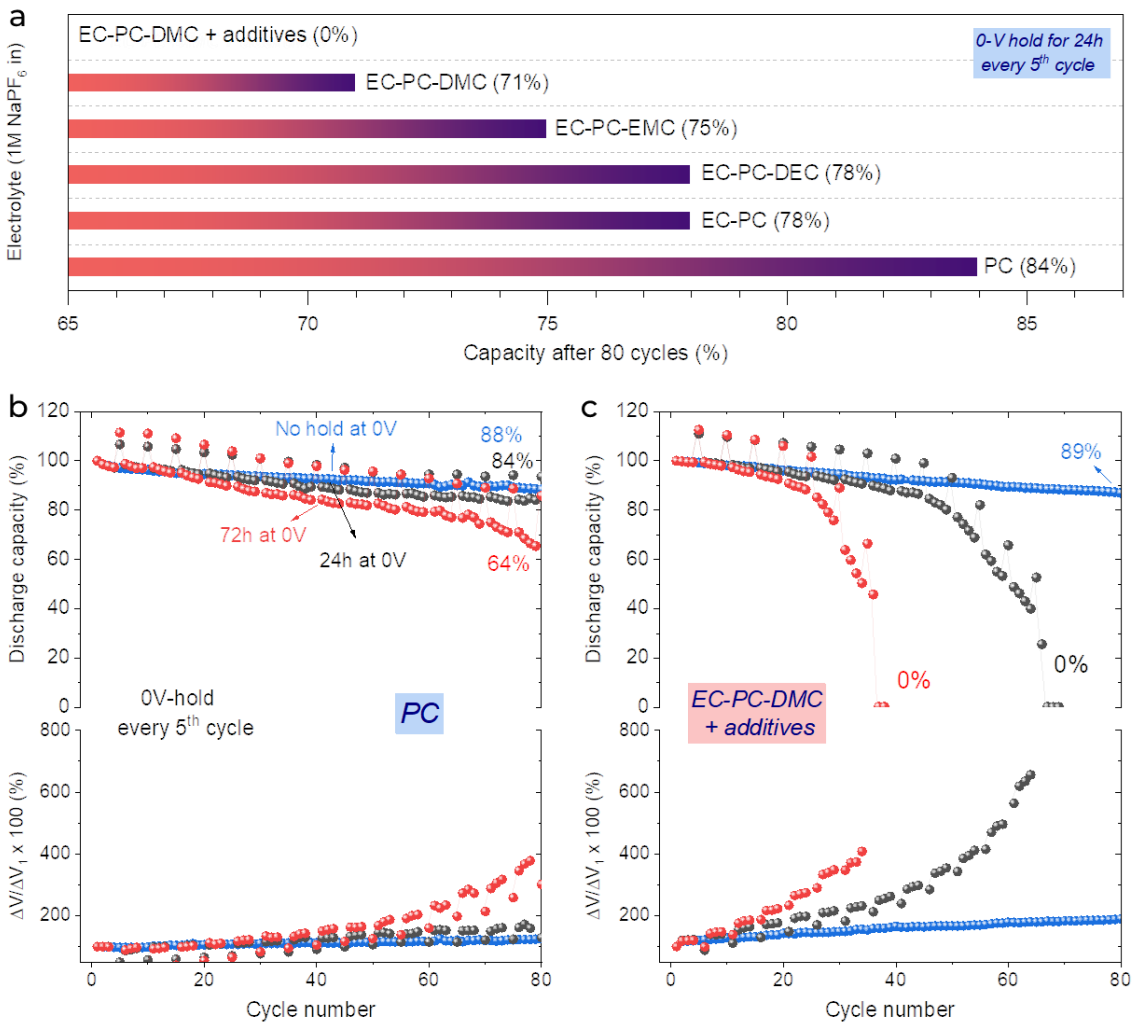

Figure 7. *(a) Comparison of capacity retained in NVPF-HC cells using different electrolyte formulations, after 80 cycles. The cells were hold at 0V for 24h after each 5 cycles between 2- 4.25 V. The capacity retention plots are shown in Fig. S14. (b and c) Capacity retention (top) and polarization changes (bottom) of the NVPF-HC cell containing (b) PC based electrolyte and (c) electrolyte having 4 additives.*

3.2 Acting at the positive electrode material level.

An alternative to improve the 0V stability is to control the HC shoot-up potential as it directly controls the SEI stability. We have earlier shown that the 3rd Na in NVPF can be electrochemically activated,[27] leading to the disordered structure and relatively sloppy profile with a low voltage plateau at ~1V (shown in Figure 8a), hence offering an opportunity to limit the HC potential shoot-up to ~1V. This hypothesis is experimentally confirmed by the excellent capacity retention of 81% (as compared to 71% retention with 2 Na removal) for 24h 0V-hold every 5th cycle in EC-PC-DMC based electrolyte displayed by NVPF-HC cells that have been highly oxidized (e.g Na content <1 in the charged state). However, prior to develop this approach, it remains to ensure that the electrolyte additives required for long calendar/cycle life that won't hamper the 0V stability.

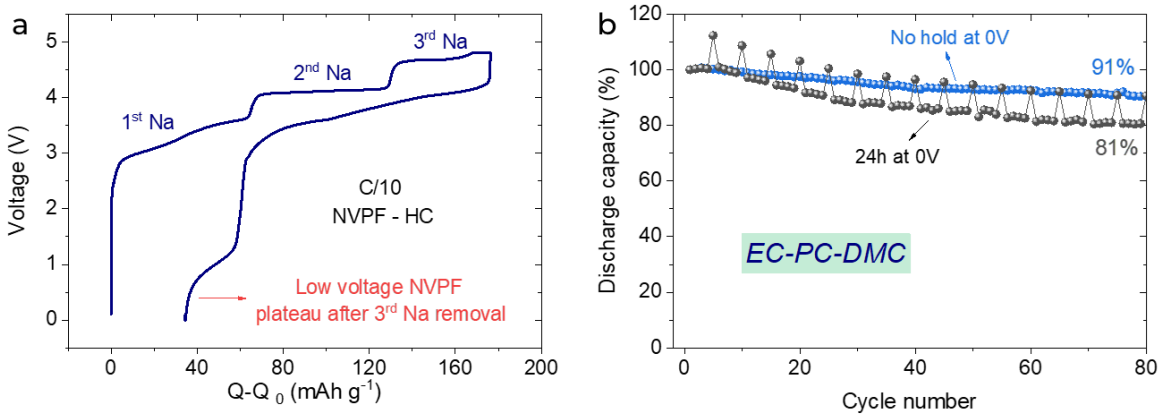

Figure 8. *(a) Cycling profile of NVPF- HC cells where the third sodium from NVPF is extracted by oxidizing to high potentials of ~4.8 V. The removal of third sodium leads to structural changes in NVPF hence changing the cycling profile in the following discharge where a low voltage redox (~1V) is observed. (b) Capacity retention plots of NVPF-HC cells cycled using 3 Na, without any 0V hold/ interruptions and with 0V hold for 24h every 5cycles.*

In a second approach we replaced the NVPF positive electrode with a sodium layered oxide $NaNi_{0.45}Zn_{0.05}Mn_{0.35}Ti_{0.15}O_2$ (ZNMT)[28] that exhibits low voltage redox than NVPF. Note that, the other family of the positive electrode, prussian blue analogs exhibit biphasic cycling behavior with the average potential of close to 3.6V depending on the transition metal ion(s) in use and is expected to behave similar to NVPF.[14] In turn, the layered oxide ZNMT used here

has a large voltage window from 2.2- 4.5 V with different plateau and sloppy regions in cycling (Fig. S17). From the cycling of ZNMT-HC in three electrode cells using NVP with 50% SOC as reference, we show Figure 9a that the HC potential is raised only to 2.7V (vs. Na/Na^+) while pushing the full cell to 0V. Thus by coupling ZNMT with PC based electrolyte we could assemble ZNMT-HC Na-ion cells (Figure 9b and 9c) showing excellent capacity retention (81% and 75% for 0V-holds of 24h and 72h, respectively vs. 87% retention for no 0V hold).

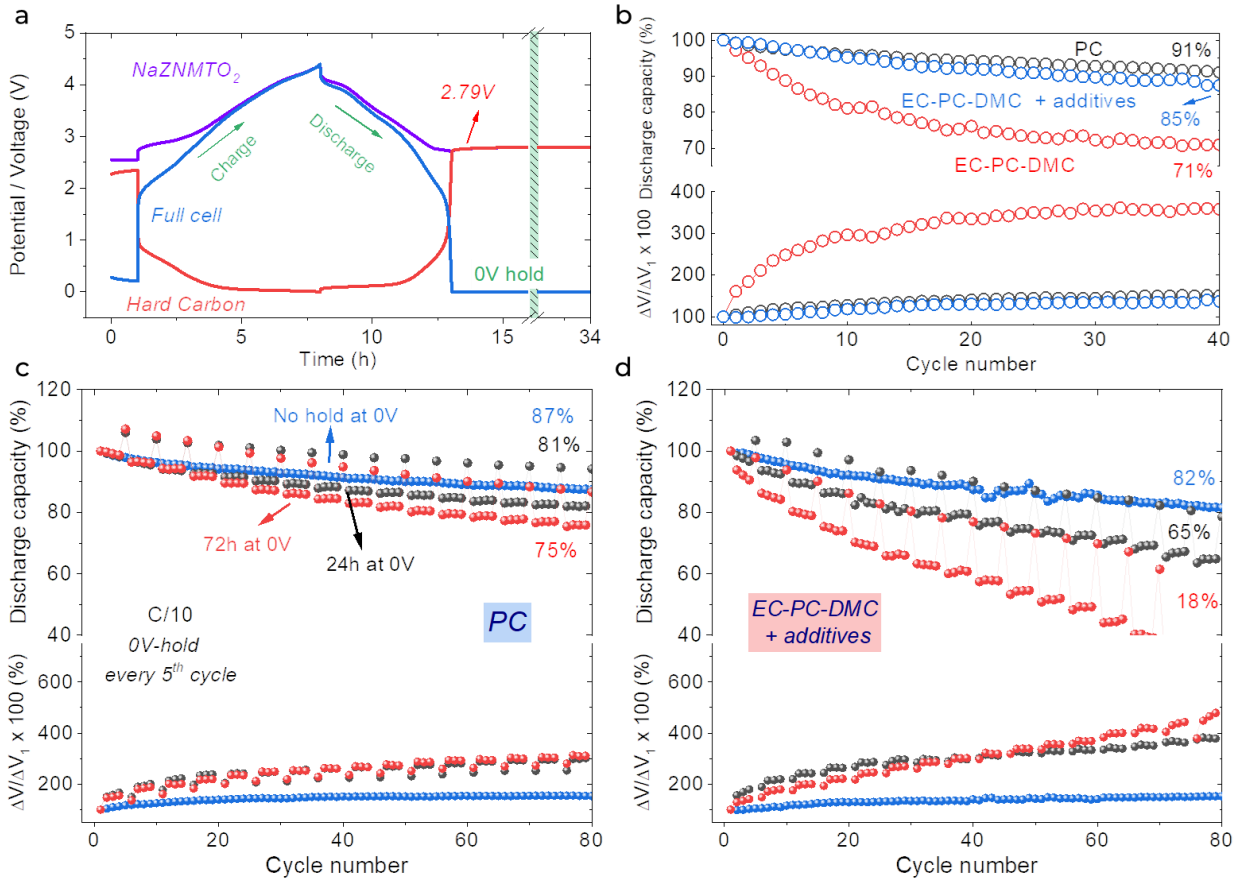

Figure 9. *(a) Cycling profile of ZNMT-HC cell in three electrode set up where NVP s used as the reference electrode. (b) Capacity retention plot of ZNMT- HC coin cells using different electrolytes. Comparative capacity retention plots of ZNMT- HC coin cells using (c) 1M $NaPF_6$ in PC and (d) 1M $NaPF_6$ in EC-PC-DMC with additives as electrolytes respectively. In both cases, the cycling is compared with and without 0V hold.*

The cycling stability of ZNMT-HC based cell with an electrolyte having linear carbonate is poor even without any 0V hold and it could be improved using electrolytes containing additives (Figure 9b). By using the electrolyte formulation with 4 additives (SN, VC, NaODFB and TMSPi)

described for NVPF study,[18] the ZNMT-HC retains the 65% and 18% capacity after 80 cycles of 24h and 72h 0V-hold in every 5th cycle, respectively. For the same electrolyte, the NVPF-HC cell failed to 0% capacity from platting. Such better stability for ZNMT-HC is simply rooted in the lower shoot-up of HC and consequently fewer side reactions. In short, the sodium layered oxides that show low voltage redox are more optimal for 0V stability, provided a suitable electrolyte is coupled with it. However, this better performance with layered oxide comes with the expense of having moisture sensitive positive electrodes and ZNMT/HC Na-ion cells of limited cycle life and power rate capability when compared to NVPF/HC Na-ion cells.

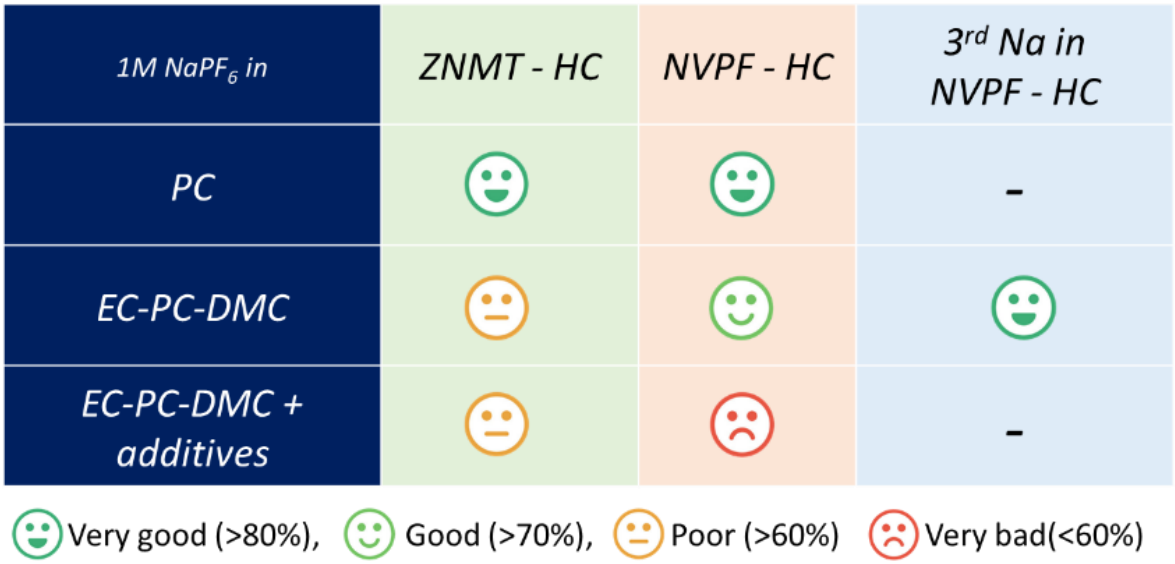

Figure 10: Comparison chart cumulating the various Na-ion systems (NVPF- HC and ZNMT- HC) studied using different electrolyte formulations. The mentioned percentage values refer to the retention after 80 cycles for 24h 0V-hold every 5 cycles protocol.

Conclusion:

We have reported the 0V stability of sodium ion systems differing by the nature of the positive electrode or of the electrolyte. We found the best performances (Figure 10) when either sodium layered oxides or NVPF are combined with PC based electrolyte and equally with highly oxidized NVPF in EC-PC-DMC based electrolyte, with the latter being the most attractive in terms of system performances. However, owing to the presence of linear carbonate (DMC), that is

known to be detrimental for high temperature performances, suitable electrolyte additives will be required to stabilize the SEI and CEI and render this solution more practical. Nevertheless, through this study we have established important observations-facts-correlations regarding zero volt stability that could be worthy of consideration for battery scientists and users depending upon the application targeted. They are,

- Usage of sodium-ion batteries in a 100% state of discharge or discharging the Na-ion cells to 0V is safer in comparison to Li-ion cells as there is no oxidation/ dissolution of the current collector in use (Al in NIBs vs. Cu in LIBs).
- Upon 0V discharge, decomposition and degradation of SEI on HC occurs and the process is exothermic.
- Repeated shorting of cell or holding at 0V leads to continuous decomposition and recreation of SEI which is more resistive with the eventual feasibility to reach sodium metal plating and rollover cell failure.
- Efficacy of the build-in SEI towards 0V discharge depends on the nature of the electrolyte used together with the potential at which the negative electrode will be brought during 0V holding. As a result, high voltage positive electrodes such as $Na_3V_2(PO_4)_2F_3$ that cycle within high voltage bi-phasic processes (3.6 and 4.2 V) show faster deterioration compared to sodium layered oxides such as O3 $NaNi_{0.5}Mn_{0.5}O_2$ where the material shows low voltage redox process around ~2.5V.
- Feasibility to optimize electrolyte with properly designed electrode chemistry could be used to reduce the cell deterioration during 0V discharge and storage.

Altogether, these results indicate that the full utilization of 0V stability in Na-ion systems requires a harmonious tuning of the combined electrode-electrolytes with the best combination varying depending upon the envisioned application. However, achieving 0V stability while not compromising other figures of merits such as energy density, power capability, and high temperature performance is challenging. The proposed mechanism of SEI dissolution and regrowth to account for our results opens up the playground to study additives which can form SEI that is stable at high HC potentials. Moreover, we show that the occasionally encountered

HC potential shoot up could be circumvented through adjusting the slippage by either pre-sodiation or sacrificial salts, etc. We hope that the present study and the knowledge gained will generate great interest among the battery community, as the 0V stability in future battery technologies will become more important than ever.

Resource Availability

Materials Availability

This study did not generate new unique reagents.

Data and Code Availability

This study did not generate any datasets.

SUPPLEMENTAL INFORMATION

Supporting note 1 explains the calculation of cell polarization during continuous cycling.

Supporting Figures S1 to S17 are additional figures for capacity retention, polarization, cyclic voltammetry of SEI stability etc.

Supporting Table S1 cumulates the XPS data.

ACKNOWLEDGMENTS

The authors thank the RS2E Network for funding as well as the financial support of Région Nouvelle Aquitaine, of the French National Research Agency (STORE-EX Labex Project ANR-10-LABX-76-01). S. M acknowledges Horizon 2020 research and innovation program under grant agreement No 875629- NAIMA. P. D thanks RS2E for PhD funding. TIAMAT, France is gratefully acknowledged for providing the NVPF/HC 18650 cells as well as the NVPF, HC electrodes for the coin cell studies.

DECLARATION OF INTERESTS

The authors declare no competing interests.

REFERENCES*

[1] JM Tarascon, The Li-Ion Battery: 25 Years of Exciting and Enriching Experiences, Interface Magazine. 25 (2016) 79–83. https://doi.org/10.1149/2.f08163if.

[2] W. Chen, J. Liang, Z. Yang, G. Li, A Review of Lithium-Ion Battery for Electric Vehicle Applications and Beyond, Energy Procedia. 158 (2019) 4363–4368. https://doi.org/10.1016/j.egypro.2019.01.783.

[3] IATA 2021 Lithium Battery Guidance Document, 2021.

[4] H. Huo, Y. Xing, M. Pecht, B.J. Züger, N. Khare, A. Vezzini, Safety Requirements for Transportation of Lithium Batteries, Energies . 10 (2017). https://doi.org/10.3390/en10060793.

[5] Federal Aviation administration, Lithium battery incidents chart, (2022). https://www.faa.gov/hazmat/resources/lithium-battery-incident-chart (accessed May 23, 2022).

[6] H. Maleki, J.N. Howard, Effects of overdischarge on performance and thermal stability of a Li-ion cell, Journal of Power Sources. 160 (2006) 1395–1402. https://doi.org/10.1016/j.jpowsour.2006.03.043.

[7] M. Zhao, S. Kariuki, H.D. Dewald, F.R. Lemke, R.J. Staniewicz, E.J. Plichta, R.A. Marsh, Electrochemical stability of copper in lithium-ion battery electrolytes, Journal of the Electrochemical Society. 147 (2000) 2874–2879. https://doi.org/10.1149/1.1393619.

[8] A. Rudola, A.J.R. Rennie, R. Heap, S.S. Meysami, A. Lowbridge, F. Mazzali, R. Sayers, C.J. Wright, J. Barker, Commercialisation of high energy density sodium-ion batteries: Faradion's journey and outlook, Journal of Materials Chemistry A. 9 (2021) 8279–8302. https://doi.org/10.1039/D1TA00376C.

[9] J.-M. Tarascon, Na-ion versus Li-ion Batteries: Complementarity Rather than Competitiveness, Joule. 4 (2020) 1616–1620. https://doi.org/10.1016/j.joule.2020.06.003.

[10] J.B.J. Wright, Storage and/or transportation of sodium-ion cells, WO2016027082A1, 2016.

[11] A. Rudola, C.J. Wright, J. Barker, Reviewing the Safe Shipping of Lithium-Ion and Sodium-Ion Cells: A Materials Chemistry Perspective, Energy Material Advances. 2021 (2021) 9798460. https://doi.org/10.34133/2021/9798460.

[12] I. Hasa, S. Mariyappan, D. Saurel, P. Adelhelm, A.Y. Koposov, C. Masquelier, L. Croguennec, M. Casas-Cabanas, Challenges of today for Na-based batteries of the future: From materials to cell metrics, Journal of Power Sources. 482 (2021) 228872. https://doi.org/10.1016/j.jpowsour.2020.228872.

[13] K. Wu, X. Dou, X. Zhang, C. Ouyang, The sodium-ion battery: An energy-storage technology for a carbon-neutral world, Engineering. (2022). https://doi.org/10.1016/j.eng.2022.04.011.

[14] A. Bauer, J. Song, S. Vail, W. Pan, J. Barker, Y. Lu, The Scale-up and Commercialization of Nonaqueous Na-Ion Battery Technologies, Advanced Energy Materials. 8 (2018) 1702869. https://doi.org/10.1002/aenm.201702869.

[15] S. Mariyappan, Q. Wang, J.M. Tarascon, Will Sodium Layered Oxides Ever Be Competitive for Sodium Ion Battery Applications?, Journal of The Electrochemical Society. 165 (2018) A3714–A3722. https://doi.org/10.1149/2.0201816jes.
[16] J. Huang, X. Han, F. Liu, C. Gervillié, L.A. Blanquer, T. Guo, J.-M. Tarascon, Monitoring battery electrolyte chemistry via in-operando tilted fiber Bragg grating sensors, Energy & Environmental Science. 14 (2021) 6464–6475. https://doi.org/10.1039/D1EE02186A.
[17] J. Huang, L. Albero Blanquer, J. Bonefacino, E.R. Logan, D. Alves Dalla Corte, C. Delacourt, B.M. Gallant, S.T. Boles, J.R. Dahn, H.-Y. Tam, J.-M. Tarascon, Operando decoding of chemical and thermal events in commercial Na(Li)-ion cells via optical sensors, Nature Energy. 5 (2020) 674–683. https://doi.org/10.1038/s41560-020-0665-y.
[18] P. Desai, J. Huang, H. Hijazi, L. Zhang, S. Mariyappan, J.-M. Tarascon, Deciphering Interfacial Reactions via Optical Sensing to Tune the Interphase Chemistry for Optimized Na-Ion Electrolyte Formulation, Advanced Energy Materials. 11 (2021) 2101490. https://doi.org/10.1002/aenm.202101490.
[19] R. Guo, L. Lu, M. Ouyang, X. Feng, Mechanism of the entire overdischarge process and overdischarge-induced internal short circuit in lithium-ion batteries, Sci Rep. 6 (2016) 30248. https://doi.org/10.1038/srep30248.
[20] X. Ma, J.E. Harlow, J. Li, L. Ma, D.S. Hall, S. Buteau, M. Genovese, M. Cormier, J.R. Dahn, Editors' Choice—Hindering Rollover Failure of Li[$Ni_{0.5}Mn_{0.3}Co_{0.2}$]O_2/Graphite Pouch Cells during Long-Term Cycling, Journal of The Electrochemical Society. 166 (2019) A711–A724. https://doi.org/10.1149/2.0801904jes.
[21] M. Bianchini, N. Brisset, F. Fauth, F. Weill, E. Elkaim, E. Suard, C. Masquelier, L. Croguennec, Na3V2(PO4)2F3 Revisited: A High-Resolution Diffraction Study, Chemistry of Materials. 26 (2014) 4238–4247. https://doi.org/10.1021/cm501644g.
[22] T. Broux, F. Fauth, N. Hall, Y. Chatillon, M. Bianchini, T. Bamine, J.-B. Leriche, E. Suard, D. Carlier, Y. Reynier, L. Simonin, C. Masquelier, L. Croguennec, High Rate Performance for Carbon-Coated Na3V2(PO4)2F3 in Na-Ion Batteries, Small Methods. 3 (2019) 1800215. https://doi.org/10.1002/smtd.201800215.
[23] P. Desai, J. Abou-Rjeily, J.-M. Tarascon, S. Mariyappan, Practicality of methyl acetate as a co-solvent for fast charging Na-ion battery electrolytes, Electrochimica Acta. 416 (2022) 140217. https://doi.org/10.1016/j.electacta.2022.140217.
[24] A. Ponrouch, R. Dedryvere, D. Monti, A.E. Demet, J.M. Ateba Mba, L. Croguennec, C. Masquelier, P. Johansson, M.R. Palacin, R. Dedryvère, D. Monti, A.E. Demet, J.M. Ateba Mba, L. Croguennec, C. Masquelier, P. Johansson, M.R. Palacín, Towards high energy density sodium ion batteries through electrolyte optimization, Energy Environ. Sci. 6 (2013) 2361–2369. https://doi.org/10.1039/c3ee41379a.
[25] R. Mogensen, D. Brandell, R. Younesi, Solubility of the Solid Electrolyte Interphase (SEI) in Sodium Ion Batteries, ACS Energy Lett. 1 (2016) 1173–1178.
[26] G. Yan, D. Alves-Dalla-Corte, W. Yin, N. Madern, G. Gachot, J.-M. Tarascon, Assessment of the Electrochemical Stability of Carbonate-Based Electrolytes in Na-Ion Batteries, Journal of The Electrochemical Society. 165 (2018) A1222–A1230. https://doi.org/10.1149/2.0311807jes.
[27] G. Yan, S. Mariyappan, G. Rousse, Q. Jacquet, M. Deschamps, R. David, B. Mirvaux, J.W. Freeland, J.-M. Tarascon, Higher energy and safer sodium ion batteries via an

electrochemically made disordered Na3V2(PO4)2F3 material, Nature Communications. 10 (2019) 585. https://doi.org/10.1038/s41467-019-08359-y.
[28] S. Mariyappan, T. Marchandier, F. Rabuel, A. Iadecola, G. Rousse, A. V Morozov, A.M. Abakumov, J.-M. Tarascon, The Role of Divalent (Zn2+/Mg2+/Cu2+) Substituents in Achieving Full Capacity of Sodium Layered Oxides for Na-Ion Battery Applications, Chemistry of Materials. 32 (2020) 1657–1666. https://doi.org/10.1021/acs.chemmater.9b05205.